Published in IET Radar, Sonar and Navigation
Received on 25th May 2010
Revised on 22nd November 2010
doi: 10.1049/iet-rsn.2010.0163

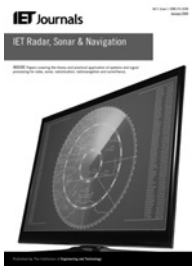

ISSN 1751-8784

# Low-angle tracking of two objects in a three-dimensional beamspace domain

*J. Kim*[1] *H.J. Yang*[2] *N. Kwak*[3]

[1]*ISR R&D Laboratory, LIG Nex1 Co., Yongin 446-798, Korea*
[2]*Department of Ocean Engineering Research, Korea Ocean Research & Development Institute, Daejeon 305-343, Korea*
[3]*Department of Electrical & Computer Engineering, Ajou University, Suwon 443-749, Korea*
*E-mail: nojunk@ajou.ac.kr*

**Abstract:** Among various low-angle tracking methods, the three-dimensional beamspace domain maximum likelihood (3-D BDML) estimation proposed by Zoltowski is a computationally attractive and optimal method that can be processed in the reduced beamspace domain. However, the estimation performance of 3-D BDML deteriorates in the presence of interference or an additional target, especially at low altitudes, because the dimension of the signal and noise exceeds the dimension provided by the three beams. This study proposes a new low-angle tracking method for two objects in a 3-D beamspace domain using a linearly constrained adaptive array. The increased signal dimension owing to the interference or the additional target is reduced in the beamspace domain by using the beamforming weight that is designed to remove the largest principal component in the covariance matrix. Numerical simulation results are provided to show the estimation performance of the proposed method.

## 1 Introduction

Low-angle tracking used to track a target flying at a low altitude has attracted a lot of interest for radar researchers. Generally, in low-angle tracking, two or more echoes return to the radar via direct and reflected paths [1] and the reflected echoes consist of specular and diffuse components [2]. If the grazing angle is small and the reflecting surface is smooth, the specular component dominates, which makes the low-angle tracking a complicated problem because of the following reasons: (i) two echoes (the direct and the specular echoes) are basically the same signal except that only the phase and the amplitude of the specular echo are different in fixed amounts from those of the direct echo; that is, they are coherent; (ii) the two echoes lie within the beamwidth, and hence, the angular separation between the two is small [3]; (iii) the two echoes are superpositioned in time, because the two echoes travel almost the same path length, and therefore the range difference between the two echoes are less than the range resolution of the radar [4]. In addition to the specular component, although it may be small, the diffuse component also complicates the low-angle tracking by adding incoherent interference to the received data [5].

In order to solve the low-angle tracking problem, various methods with different approaches have been proposed, which can be classified into three main families; that is, the mono-pulse methods, the parametric estimations and the subspace-based methods [4, 6]. Firstly, the mono-pulse methods utilise the ratio of the sum channel to the difference channel, and hence, they are computationally the simplest [7]. However, they have a limit in that they cannot track an elevation angle of less than one-fourth of the beamwidth [8]. Secondly, the parametric estimations are generally based on the maximum likelihood (ML) estimator. They are less sensitive to signal coherence and usually have lower Cramér–Rao bounds than those of the other methods [9]. However, they require statistical information about signals, and a lot of computations are needed in performing a multidimensional grid search [6]. Thirdly, the subspace-based methods, such as the multiple signal classification (MUSIC) [10], estimate the direction of arrival (DOA) by solving a spectrum-like function related to the orthogonality between the signal subspace and the noise subspace of the covariance matrix, and therefore, the subspace-based methods are computationally more attractive than parametric methods [6]. However, the accuracy of the subspace-based methods is inferior to that of the parametric methods especially when the signals are coherent. This performance degradation due to the signal coherence can be alleviated by the use of spatial smoothing or generalised covariance differencing along with the MUSIC method [11–13]. However, an estimation bias is inevitable in those methods.

In the subspace-based methods, the array output is transformed from elementspace to beamspace with the pre-multiplication by the beamforming weight, and it is often advantageous to process the estimation in the beamspace domain than in the elementspace domain [14]. By the beamspace processing, the spatial domain is divided into several spatial bands. The spatial band spotlighted by beams is termed as in-band, and the other spatial band is

termed as out-of-band [15]. Since signals are coming from a low angle, it is possible to accentuate the in-band signal of interest by steering beams to low angle and performing the estimation in the beamspace domain. Therefore the beamspace processing provides more accurate localisation of the in-band signal than the elementspace processing especially when there exists a dispersed interference such as diffuse reflection or clutter return in the out-of-band (see Fig. 1). Furthermore, the computational complexity can be reduced because there exists a closed-form solution that can be found without a search process [16, 17]. Among the beamspace domain methods, a number of methods employing three beams have been proposed for low-angle tracking [18, 19]. Note that under ideal assumptions, the estimation performance in the 3-D beamspace domain does not degrade, because a 3-D observation vector is enough to distinguish three different spaces, two for the signals (direct and specular echoes) and one for the noise. The most notable work on 3-D beamspace domain estimation is the 3-D beamspace domain maximum likelihood (3-D BDML) estimation for its simplicity [20]. In the 3-D BDML estimation, three $M$-dimensional orthogonal beamforming weights which have $(M-3)$ common nulls are used, where $M$ denotes the number of array elements. Therefore any combination of these three beamforming weights has the same nulls as the aforementioned $(M-3)$ common nulls. Since $(M-1)$ nulls exist in total, the two remaining nulls can be used to find the two echoes. With this feature, 3-D BDML offers closed-form solutions for the two echo angles, and thus it is extremely simple in computational complexity.

On the other hand, the 3-D BDML method is susceptible to deviations from the ideal assumptions. In particular, in the presence of a point interference from low altitudes, such as a jammer, as well as the two echoes from the target, the dimension of the subspace to be distinguished increases [21]; hence, the estimation performance of the 3-D BDML method degrades severely. This is owing to the number of dimensions provided by the 3-D beamspace observation being not enough to distinguish more than three components (two from a target and one from the noise) [22]. The same problem arises in the presence of an additional low-angle target [As a point interference and a secondary target has the same effect, henceforth, we will use the term 'secondary object' for both. On the other hand, the term 'primary object' will be used to denote the original target.]. To tackle this problem, we may naively increase the dimensionality of the beamspace by using more beams. However, the additional beams used to procure more dimensions are placed beside the original three beams, facing out of the boresight. Therefore the suppressed out-of-band interference can enter the in-band region of the additional beams, as shown in Fig. 1. Moreover, if the out-of-band interference is dispersed, then it cannot be localised with the addition of beams. Therefore the estimation error is increased.

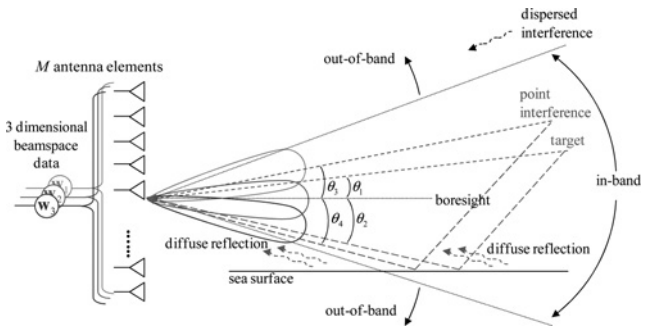


**Fig. 1** *Three beams used for the low-angle tracking*

In this paper, we propose a low-angle tracking algorithm for two objects (primary and secondary) in the three-dimensional (3-D) beamspace domain to minimise the estimation error. We design the three beams so that, out of total $(M-1)$ nulls, they have $(M-5)$ nulls fixed in common, and leave the other four variable nulls to find a pair of coherent signals while nullifying the other pair of coherent signals; for example, two echoes through the direct and specular paths owing to a jamming signal from other ship. In the proposed method, one of the two objects (a jammer or a target) is removed in the beamspace domain data by designing the beamforming weights to eliminate the largest principal component (LPC) of the covariance matrix utilising variable nulls. Therefore only a pair of coherent signal components from two directions remain in the beamspace domain data, which can be distinguished with three beams. Furthermore, the two DOAs of the removed object can also be estimated in the end, by utilising the properties of the beamforming weights. Therefore, all the DOAs from the two objects are finally estimated. The proposed algorithm shows a better estimation accuracy than the conventional methods such as the 3-D BDML estimation and the beamspace root-MUSIC method [17] in the presence of a secondary object along with dispersed out-of-band interference.

This paper is organised as follows: In Section 2, the signal model and the estimation procedure found in the conventional 3-D BDML method are described. In Section 3, the signal model of two objects are provided and the shortcomings of the conventional 3-D BDML method are also presented. Then, the proposed method is described. Firstly, the proposed beamforming process which is used to generate the desired beamforming weights is described. Secondly, the procedure to estimate the DOA is provided. The numerical simulation results as well as the comparison with the conventional methods are provided in Section 4. Finally, we summarise and conclude this paper in Section 5.

## 2 Conventional 3-D BDML method

To ensure the completeness of the paper, the overall procedure of the 3-D BDML method is briefly reviewed. First, let us examine the low-angle tracking signal model. In the 3-D BDML method, they consider a uniform linear array (ULA) of $M$ elements in the presence of two echoes from a primary object. Here, we assume that the direct echo is incoming from $\theta_1$ and the specular echo is incoming from $\theta_2$, as depicted in Fig. 1. The diffuse component is neglected in the 3-D BDML method because the smooth sea surface and low grazing angle are assumed. The $n$th snapshot of the total $N$ samples of received data is denoted by $M$-dimensional complex vector, $\boldsymbol{x}$, which can be expressed as

$$\begin{aligned}\boldsymbol{x}(n) &= s_1(n)\boldsymbol{a}(\phi_1) + s_2(n)\boldsymbol{a}(\phi_2) + \boldsymbol{n}(n) \\ &= \boldsymbol{A}(\boldsymbol{\phi})\boldsymbol{s}(n) + \boldsymbol{n}(n), \quad n = 1, \ldots, N \end{aligned} \tag{1}$$

where the two elements of $\boldsymbol{s}(n) \triangleq [s_1(n)\ s_2(n)]^{\mathrm{T}}$ are the complex envelopes of a direct and a specular echo signal,




doi: 10.1049/iet-rsn.2010.0163

respectively, at the sample sequence $n$. These two signals are coherent because one is a reflection of the other, that is, $s_2(n) = \rho_1 e^{j\Delta\psi_{12}} s_1(n)$, where $\rho_1$ is the magnitude of the reflection coefficient and $\Delta\psi_{12}$ is the phase difference between $s_1(n)$ and $s_2(n)$. Furthermore, the unmeasurable additive noise is denoted by $\boldsymbol{n}(n)$ and assumed to be white Gaussian. The $i$th column vector of the $M \times 2$ matrix $\boldsymbol{A}(\boldsymbol{f}) \triangleq [\boldsymbol{a}(\phi_1)\ \boldsymbol{a}(\phi_2)]$ is an array response vector of the $i$th element of $\boldsymbol{A}(\boldsymbol{\phi}) \triangleq [\boldsymbol{a} \cdots$ and $\boldsymbol{\phi} \triangleq]$, which can be expressed as

$$\boldsymbol{a}(\phi_i) = [e^{-j(M/2-1/2)\phi_i},\ e^{-j(M/2-3/2)\phi_i},\ \ldots,\ e^{j(M/2-3/2)\phi_i},\ e^{j(M/2-1/2)\phi_i}]^{\mathrm{T}} \tag{2}$$

Here, $\phi_i = 2\pi(L_0/\lambda)\sin\theta_i$, where $L_0$ is the distance between the array elements and $\lambda$ is the wavelength. Note that the array response vector is defined with the assumption that the phase of the centre of the array is zero. Therefore the array response vector is conjugate centro-symmetric; that is, each element of the array response vector is the complex conjugate of the element symmetric with respect to the centre of the array. The conjugate centro-symmetric property is necessary to localise coherent signals, and this statement is examined thoroughly later in this section.

From the received data vector $\boldsymbol{x}$, the beamspace data $\boldsymbol{x}_{\mathrm{B}}$ are obtained by multiplying the predefined beamforming weight matrix $\boldsymbol{W}$ as follows

$$\boldsymbol{x}_{\mathrm{B}}(n) = \boldsymbol{W}^H \boldsymbol{x}(n) = \boldsymbol{D}(\boldsymbol{\phi})\boldsymbol{s}(n) + \boldsymbol{W}^H \boldsymbol{n}(n) \tag{3}$$

Here, $\boldsymbol{W} \triangleq [\boldsymbol{w}_1\ \boldsymbol{w}_2\ \boldsymbol{w}_3]$ is an $M \times 3$ matrix, whose column represents the individual beamforming weight of the three beams and $()^H$ denotes the conjugate transpose. In addition, we define a $3 \times 2$ matrix, $\boldsymbol{D}(\boldsymbol{\phi})$ as $\boldsymbol{D}(\boldsymbol{\phi}) \triangleq [\boldsymbol{d}(\phi_1)\ \boldsymbol{d}(\phi_2)] = \boldsymbol{W}^H \boldsymbol{A}(\boldsymbol{\phi})$ for the sake of simplicity. Even though the size of received data increases in proportion to the array size $M$, that of the beamspace data remains three because three beams are employed.

The least square estimations of $\phi_1$, $\phi_2$ and $s(1), \ldots, s(N)$ can be formulated as

$$\min_{\phi_1,\phi_2,s(1),\ldots,s(N)} \sum_{n=1}^{N} \|\boldsymbol{x}_{\mathrm{B}} - \boldsymbol{D}(\boldsymbol{\phi})\boldsymbol{s}(n)\|^2 \tag{4}$$

In the 3-D BDML method, the discrete Fourier transform (DFT) beamforming weights are employed, which can be expressed as

$$\boldsymbol{W} = \left[\boldsymbol{a}\left(-\frac{2\pi}{M}\right)\ \boldsymbol{a}(0)\ \boldsymbol{a}\left(\frac{2\pi}{M}\right)\right] \tag{5}$$

where $\boldsymbol{a}(\phi)$ is defined in (2). As the noise $\boldsymbol{n}(n)$ is assumed to be white Gaussian, (4) also corresponds to the ML estimation because the beamforming weights are mutually orthogonal. For the purpose of estimating $\phi_1$ and $\phi_2$, we first estimate $\boldsymbol{s}(n)$ and then estimate $\boldsymbol{D}(\boldsymbol{\phi})$ utilising the separability property of $\boldsymbol{s}(n)$ and $\boldsymbol{\phi}$. Regardless of $\boldsymbol{\phi}$, the least square solution for $\mathbf{s}(n)$ is $\hat{\mathbf{s}}_{\mathrm{LS}} = [\boldsymbol{D}^H(\boldsymbol{\phi})\boldsymbol{D}(\boldsymbol{\phi})]^{-1}\boldsymbol{D}^H(\boldsymbol{\phi})\boldsymbol{x}_{\mathrm{B}}$. Substituting this for $\mathbf{s}(n)$ in (4), we obtain

$$\min_{\phi_1,\phi_2} \sum_{n=1}^{N} \boldsymbol{x}_{\mathrm{B}}^H(n)\boldsymbol{P}(\boldsymbol{\phi})\boldsymbol{x}_{\mathrm{B}}(n) \tag{6}$$

where

$$\boldsymbol{P}(\boldsymbol{\phi}) = \boldsymbol{I}_3 - \boldsymbol{D}(\boldsymbol{\phi})[\boldsymbol{D}^H(\boldsymbol{\phi})\boldsymbol{D}(\boldsymbol{\phi})]^{-1}\boldsymbol{D}^H(\boldsymbol{\phi}) \tag{7}$$

Here, $\boldsymbol{I}$ is the 3-D identity matrix. Note that $\boldsymbol{P}(\boldsymbol{\phi})$ is the orthogonal projector of $\boldsymbol{x}_{\mathrm{B}}(n)$ onto the $1-D$ noise subspace orthogonal to the span of $\boldsymbol{D}(\boldsymbol{\phi})$. Hence, the $1-D$ projector can be modelled as

$$\boldsymbol{P}(\boldsymbol{\phi}) = \frac{\boldsymbol{v}(\boldsymbol{\phi})\boldsymbol{v}^H(\boldsymbol{\phi})}{\boldsymbol{v}^H(\boldsymbol{\phi})\boldsymbol{v}(\boldsymbol{\phi})} \tag{8}$$

where $\boldsymbol{v}(\boldsymbol{\phi})$ is a $3 \times 1$ vector that satisfies

$$\boldsymbol{v}^H(\boldsymbol{\phi})\boldsymbol{D}(\boldsymbol{\phi}) = 0 \tag{9}$$

At this point, we consider the condition of the beamforming weight. Recall that the array response vector in (2) is given to be conjugate centro-symmetric. Therefore if each beamforming weight in $\boldsymbol{W}$ is also designed to be conjugate centro-symmetric, all the elements of $\boldsymbol{D}(\boldsymbol{\phi})$, $\boldsymbol{P}(\boldsymbol{\phi})$ and $\boldsymbol{v}(\boldsymbol{\phi})$ become real valued. After substituting $\boldsymbol{P}(\boldsymbol{\phi})$ in (6) with (8), we can convert (6) from the optimisation problem over $\boldsymbol{\phi}$ to an optimisation problem over the real-valued vector $\boldsymbol{v}(\boldsymbol{\phi})$ by the following manipulation

$$\begin{aligned}
&\min_{\boldsymbol{v}(\boldsymbol{\phi})} \frac{\sum_{n=1}^{N} x_{\mathrm{B}}^H(n)\boldsymbol{v}(\boldsymbol{\phi})\boldsymbol{v}(\boldsymbol{\phi})^{\mathrm{T}}x_{\mathrm{B}}(n)}{\boldsymbol{v}(\boldsymbol{\phi})^{\mathrm{T}}\boldsymbol{v}(\boldsymbol{\phi})} \\
&= \min_{\boldsymbol{v}(\boldsymbol{\phi})} \frac{\sum_{n=1}^{N} \mathrm{Re}[x_{\mathrm{B}}^H(n)\boldsymbol{v}(\boldsymbol{\phi})\boldsymbol{v}(\boldsymbol{\phi})^{\mathrm{T}}x_{\mathrm{B}}(n)]}{\boldsymbol{v}(\boldsymbol{\phi})^{\mathrm{T}}\boldsymbol{v}(\boldsymbol{\phi})} \\
&= \min_{\boldsymbol{v}(\boldsymbol{\phi})} \frac{\sum_{n=1}^{N} \mathrm{Re}[\boldsymbol{v}(\boldsymbol{\phi})^{\mathrm{T}}x_{\mathrm{B}}(n)x_{\mathrm{B}}^H(n)\boldsymbol{v}(\boldsymbol{\phi})]}{\boldsymbol{v}(\boldsymbol{\phi})^{\mathrm{T}}\boldsymbol{v}(\boldsymbol{\phi})} \\
&= \min_{\boldsymbol{v}(\boldsymbol{\phi})} N \frac{\boldsymbol{v}(\boldsymbol{\phi})^{\mathrm{T}}\,\mathrm{Re}\,[\hat{\boldsymbol{R}}_{bb}]\boldsymbol{v}(\boldsymbol{\phi})}{\boldsymbol{v}(\boldsymbol{\phi})^{\mathrm{T}}\boldsymbol{v}(\boldsymbol{\phi})}
\end{aligned} \tag{10}$$

In the last line, $\hat{\boldsymbol{R}}_{bb}$ denotes the beamspace domain sample covariance matrix; that is

$$\hat{\boldsymbol{R}}_{bb} = \frac{1}{N}\sum_{n=1}^{N} \boldsymbol{x}_{\mathrm{B}}\boldsymbol{x}_{\mathrm{B}}^H \tag{11}$$

The solution of (10) for $\boldsymbol{v}(\boldsymbol{\phi})$ is the eigenvector associated with the smallest eigenvalue of $\mathrm{Re}[\hat{\boldsymbol{R}}_{bb}]$. The 3-D BDML uses $\mathrm{Re}[\hat{\boldsymbol{R}}_{bb}]$ because, in the presence of a pair of coherent signals, $1-D$ noise subspace can be distinguished by the eigendecomposition of $\mathrm{Re}[\hat{\boldsymbol{R}}_{bb}]$ rather than that of $\hat{\boldsymbol{R}}_{bb}$ [20]. Note here that the equality in the last line of (10) holds because the projection vector $\boldsymbol{v}(\boldsymbol{\phi})$ is a real vector, which follows from the fact that the beamforming weight is conjugate centro-symmetric. Therefore it should be noted that the use of the conjugate centro-symmetric beamforming weight is important to localise coherent signals.

Let us denote the solution found in (10) as $\boldsymbol{v}$, then, from (9) we obtain

$$\boldsymbol{v}^{\mathrm{T}}\boldsymbol{d}(\phi_i) = \boldsymbol{v}^{\mathrm{T}}\boldsymbol{W}^H\boldsymbol{a}(\phi_i) = 0, \quad i = 1, 2 \tag{12}$$

Substituting $e^{j\phi_i}$ in $\boldsymbol{a}(\phi_i)$, which is defined in (2), with $z_i$, we get an $(M-1)$th degree polynomial equation of $z_i$. We can estimate $\phi_i$ by solving this polynomial equation. In the 3-D

BDML method, $(M-3)$ common nulls exist in each column of $\boldsymbol{W}$. These common nulls can be factored out, and hence, we have only to solve the remaining second-order polynomial. With this feature, 3-D BDML offers closed-form solutions for the two echo angles. Therefore 3-D BDML is extremely simple in computational complexity. In summary, the overall procedure of the conventional 3-D BDML is depicted in Fig. 2.

## 3 Proposed estimation method

The estimation performance of the 3-D BDML method degrades severely, in the presence of a secondary object at low altitude. In this section, we propose an estimation method based on three beams, which performs nicely in the presence of a secondary object. First, the signal model of the two objects is represented in the next subsection. The performance degradation of 3-D BDML in the presence of two objects is also examined. Then, we describe each step of the proposed method in detail. The beamforming and the estimation of the proposed method are examined in the subsequent subsections.

### 3.1 Signal model of two objects

In the presence of a secondary object such as a point interference or an additional target, the spatially correlated component [23] is added to the signal model of 3-D BDML, and hence, the number of signals increases from two to four. Therefore the signal model (1) is modified to

$$\begin{aligned}\boldsymbol{x}(n) &= s_1(n)\boldsymbol{a}(\phi_1) + s_2(n)\boldsymbol{a}(\phi_2) + s_3(n)\boldsymbol{a}(\phi_3) \\ &\quad + s_4(n)\boldsymbol{a}(\phi_4) + \boldsymbol{n}(n) \\ &= \boldsymbol{A}(\boldsymbol{\phi})\boldsymbol{s}(n) + \boldsymbol{n}(n), \quad n = 1, \ldots, N \end{aligned} \tag{13}$$

Here, $\boldsymbol{s}(n)$ is modified to

$$\boldsymbol{s}(n) \triangleq [s_1(n)\ s_2(n)\ s_3(n)\ s_4(n)]^{\mathrm{T}} \tag{14}$$

where $s_3(n)$ and $s_4(n)$ are the complex envelope of the direct and specular echoes of the secondary object, respectively. Thus, $s_4(n) = \rho_3 \mathrm{e}^{\mathrm{j}\Delta\psi_{34}} s_3(n)$ where $\rho_3$ is the magnitude of the reflection coefficient related to the secondary object and $\Delta\psi_{34}$ is the phase difference between $s_3(n)$ and $s_4(n)$. Similarly, the number of columns in $\boldsymbol{A}(\boldsymbol{\phi})$ also increases from two to four. Hence, we obtain

$$\boldsymbol{A}(\boldsymbol{\phi}) = [\boldsymbol{a}(\phi_1)\ \boldsymbol{a}(\phi_2)\ \boldsymbol{a}(\phi_3)\ \boldsymbol{a}(\phi_4)] \tag{15}$$

where $\boldsymbol{a}(\phi_k)$, $k = 1, \ldots, 4$, is the array response vector of $\phi_k$. This model holds for both cases of $\rho_3 = 0$ and $\rho_3 \neq 0$. The former is the case of no reflection from the secondary object, while the latter is the case where there exists a specular reflection from the secondary object.

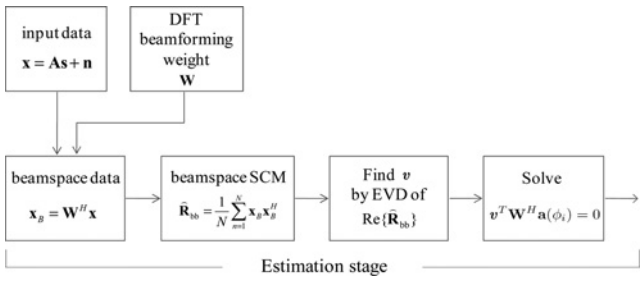


**Fig. 2** *Overall procedure in the conventional 3-D BDML method*

Now, we investigate the shortcomings of the 3-D BDML in the presence of two objects. First, in order to find the 1-D projector orthogonal to the signal subspace (see Fig. 2), we obtain the real part of the beamspace sample covariance matrix, which can be expressed as

$$\mathrm{Re}[\hat{\boldsymbol{R}}_{bb}] = \mathrm{Re}[\boldsymbol{W}^H \hat{\boldsymbol{R}}_{xx} \boldsymbol{W}] \tag{16}$$

where $\hat{\boldsymbol{R}}_{xx}$, the sample covariance matrix of $\boldsymbol{x}(n)$, is expressed as $\hat{\boldsymbol{R}}_{xx} = (1/N)\Sigma_{i=1}^{N} \boldsymbol{x}(n)\boldsymbol{x}^H(n)$. Taking the expected value of $\hat{\boldsymbol{R}}_{xx}$, the covariance matrix $\boldsymbol{R}_{xx}$ can be expressed as

$$\boldsymbol{R}_{xx} \triangleq E\{\hat{\boldsymbol{R}}_{xx}\} = \boldsymbol{A}(\boldsymbol{\phi})\boldsymbol{R}_{ss}(n)\boldsymbol{A}^H(\boldsymbol{\phi}) + \sigma_n^2 \boldsymbol{I}_M \tag{17}$$

where $E\{\}$ denotes the expectation, $\sigma_n^2$ is the noise variance, $\boldsymbol{I}_M$ is the $M \times M$ identity matrix and $\boldsymbol{R}_{\mathrm{ss}}(n)$ is the covariance matrix of $\boldsymbol{s}(n)$; that is

$$\begin{aligned}\boldsymbol{R}_{\mathrm{ss}}(n) &\triangleq E\{\boldsymbol{s}(n)\boldsymbol{s}^H(n)\} \\ &= E\{[s_1(n) \quad \rho_1 \mathrm{e}^{\mathrm{j}\Delta\psi_{12}} s_1(n) \quad s_3(n) \quad \rho_3 \mathrm{e}^{\mathrm{j}\Delta\psi_{34}} s_3(n)]^{\mathrm{T}} \\ &\quad \times [s_1^*(n) \quad \rho_1 \mathrm{e}^{-\mathrm{j}\Delta\psi_{12}} s_1^*(n) \quad s_3^*(n) \quad \rho_3 \mathrm{e}^{-\mathrm{j}\Delta\psi_{34}} s_3^*(n)]\} \end{aligned} \tag{18}$$

where $()^*$ denotes the complex conjugate. Here, direct echoes of $\boldsymbol{s}(n)$ can be represented by

$$s_i(n) = \alpha_i(n)\mathrm{e}^{\mathrm{j}\omega_i t_s n + \zeta_i}, \quad i = 1, 3 \tag{19}$$

where $\alpha_i(n)$ is the amplitude of the $n$th snapshot, $\omega_i$ is the angular frequency which is the sum of the transmit and doppler frequencies, $t_{\mathrm{s}}$ is the sampling interval, and $\zeta_{\mathrm{i}}$ is the initial phase [24]. We assume that $\alpha_i(n)$ is a random variable whose distribution is defined according to the object models in [25], and $\zeta_{\mathrm{i}}$ is a random variable uniformly distributed over $[-\pi, \pi]$. Therefore, from (19), we obtain

$$E\{s_1(n)s_1^*(n)\} = E\{\alpha_1^2(n)\} = \sigma_1^2 \tag{20}$$

$$E\{s_3(n)s_3^*(n)\} = E\{\alpha_3^2(n)\} = \sigma_3^2 \tag{21}$$

where $\sigma_1^2$ and $\sigma_3^2$ is the variance of $s_1(n)$ and $s_3(n)$, respectively, and we also obtain

$$E\{s_1(n)s_3^*(n)\} = E\{\alpha_1(n)\alpha_3(n)\mathrm{e}^{\mathrm{j}(\omega_1-\omega_3)t_s n + \zeta_1 - \zeta_3}\} = 0 \tag{22}$$

$$E\{s_3(n)s_1^*(n)\} = E\{\alpha_1(n)\alpha_3(n)\mathrm{e}^{\mathrm{j}(\omega_3-\omega_1)t_s n + \zeta_3 - \zeta_1}\} = 0 \tag{23}$$

where we assumed $\omega_1 \neq \omega_3$. From (18)–(23), we have

$$\boldsymbol{R}_{\mathrm{ss}}(n) = \begin{bmatrix} \sigma_1^2 & \sigma_1^2\rho_1 \mathrm{e}^{-\mathrm{j}\Delta\psi_{12}} & 0 & 0 \\ \sigma_1^2\rho_1 \mathrm{e}^{\mathrm{j}\Delta\psi_{12}} & \sigma_1^2\rho_1^2 & 0 & 0 \\ 0 & 0 & \sigma_3^2 & \sigma_3^2\rho_3 \mathrm{e}^{-\mathrm{j}\Delta\psi_{34}} \\ 0 & 0 & \sigma_3^2\rho_3 \mathrm{e}^{\mathrm{j}\Delta\psi_{34}} & \sigma_3^2\rho_3^2 \end{bmatrix} \tag{24}$$




doi: 10.1049/iet-rsn.2010.0163

and hence, $\boldsymbol{R}_{ss}$ does not vary with $n$ and can be expressed as

$$\boldsymbol{R}_{ss} = \sigma_1^2 \begin{bmatrix} 1 \\ \rho_1 e^{j\Delta\psi_{12}} \\ 0 \\ 0 \end{bmatrix} \begin{bmatrix} 1 & \rho_1 e^{j\Delta\psi_{12}} & 0 & 0 \end{bmatrix}^H + \sigma_3^2 \begin{bmatrix} 0 \\ 0 \\ 1 \\ \rho_3 e^{j\Delta\psi_{34}} \end{bmatrix} \begin{bmatrix} 0 & 0 & 1 & \rho_3 e^{j\Delta\psi_{34}} \end{bmatrix}^H \quad (25)$$

Therefore the rank of $\boldsymbol{R}_{ss}$ is two, even though there are four signals in $\boldsymbol{s}(n)$. This rank reduction is caused because two pairs of signals are coherent. Hence, the signal subspace of $\boldsymbol{R}_{xx}$, which is the first term of the right-hand side of (17) is also of rank two [This implies that the dimension of the signal subspace is reduced from 4 to 2 by their coherent property. Therefore all DOAs of the four signals intermingle in the rank-two signal subspace and cannot be estimated by the eigendecomposition of $\boldsymbol{R}_{xx}$.]. However, the rank of Re[$\boldsymbol{R}_{ss}$], which can be expressed as (see (26))

is larger than 2 unless both $\cos^2(\Delta\psi_{12})$ and $\cos^2(\Delta\psi_{34})$ are equal to one [This implies that the reduced dimension of the signal subspace can be restored by taking the real part of $\boldsymbol{R}_{ss}$. This is allowed because the 1-D projector defined in (8) and (10) is real valued when the beamforming weight is conjugate centro-symmetric. Thus, the conjugate centro-symmetry is an essential property in determining the beamforming weight.]. Finally, replacing $\boldsymbol{R}_{xx}$ in (16) with (17), we obtain

$$\begin{aligned} \mathrm{Re}[\boldsymbol{R}_{bb}] &= \mathrm{Re}[\boldsymbol{W}^H(\boldsymbol{A}(\boldsymbol{\phi})\boldsymbol{R}_{ss}\boldsymbol{A}^H(\boldsymbol{\phi}) + \sigma_n \boldsymbol{I}_M)\boldsymbol{W}] \\ &= \boldsymbol{W}^H\boldsymbol{A}(\boldsymbol{\phi})\mathrm{Re}[\boldsymbol{R}_{ss}]\boldsymbol{A}^H(\boldsymbol{\phi})\boldsymbol{W} + \sigma_n \boldsymbol{W}^H\boldsymbol{W} \end{aligned} \quad (27)$$

The second equality follows from the fact that $\boldsymbol{D}(\boldsymbol{\phi}) = \boldsymbol{W}^H\boldsymbol{A}(\boldsymbol{\phi})$ is real-valued when $\mathbf{W}$ is conjugate centro-symmetric. Incidentally, if the rank of $\boldsymbol{W}^H\boldsymbol{A}(\boldsymbol{\phi})$ is three, $\boldsymbol{W}^H\boldsymbol{A}(\boldsymbol{\phi})\mathrm{Re}[\boldsymbol{R}_{ss}]\boldsymbol{A}^H(\boldsymbol{\phi})\boldsymbol{W}$ in (27) becomes a full-rank matrix. Therefore the dimension of the beamspace domain is not sufficient to distinguish signals from one another, which results in an increased estimation error. This situation also applies when there is no reflection from the secondary object ($\rho_3 = 0$) because $\boldsymbol{W}^H\boldsymbol{A}(\boldsymbol{\phi})\mathrm{Re}[\boldsymbol{R}_{ss}]\boldsymbol{A}^H(\boldsymbol{\phi})\boldsymbol{W}$ is full rank.

We may increase the beamspace dimension by using more beams and exploit naively the beamspace root-MUSIC method by using the real part of the covariance matrix [17]. However, this method is not suitable for the following reasons. Firstly, the additional beams used to procure more dimensions are placed beside the original three beams and are facing out of the boresight. Therefore the in-band region is broaden and an out-of-band interference of the original three beams can be located in the in-band region of the additional beams. This makes the estimation susceptible to out-of-band interference. Secondly, the additional beams increase numerical instability. In the beamspace root-MUSIC method, a transformation matrix is defined such that a column of which represents the remaining nulls of each beamforming weight after removing nulls in common. This matrix is transformed to the beamspace root-MUSIC polynomial [17]. However, the transformation matrix becomes ill conditioned as the number of beams increases [15], which results in an increase in the estimation error. Therefore in order to solve the dimension deficiency problem, we focus on designing three beamforming weights to remove one of the signal components. This removal reduces the rank of $\boldsymbol{W}^H\boldsymbol{A}(\boldsymbol{\phi})$ to less than three.

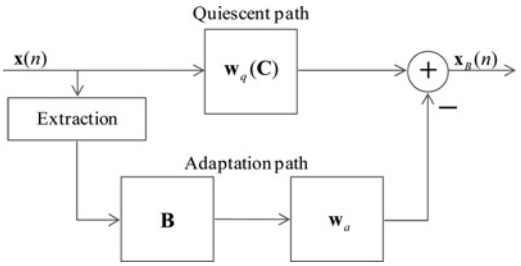


**Fig. 3** *Block diagram of the modified GSC*

### 3.2 Proposed method of beamforming

The proposed beamforming weights need to have the following three properties: (i) The beamforming weights need to reduce the dimension of signal subspace from 4 to 2 by eliminating one of the two objects in the sample covariance matrix. However, the directions of the echoes from the eliminated object also need to be estimated because this object may be the primary object to localise; (ii) The beamforming weights must have common nulls in order that the polynomial induced from (12) can be reduced to a polynomial of an order lower than five, thereby it has closed-form solutions; (iii) The beamforming weights need to be conjugate centro-symmetric.

To achieve these three properties, we propose to employ linearly constrained adaptive arrays in the form of the generalised sidelobe canceller (GSC) [26] with a modification. The modified GSC consists of the upper path (quiescent path), which is derived from the linear constraints $\boldsymbol{C}$ and generates the quiescent weight $\boldsymbol{w}_\mathrm{q}$, and the lower path (adaptation path), which generates the adaptation weight $\boldsymbol{w}_\mathrm{a}$, as depicted in Fig. 3. As the blocking matrix $\boldsymbol{B}$ is the null space of the constraint matrix $\boldsymbol{C}$, the adaptation is performed in the null space of $\boldsymbol{C}$, and hence, the weight at the GSC output, which can be expressed as

$$\boldsymbol{w}_\mathrm{G} = \boldsymbol{w}_\mathrm{q} - \boldsymbol{B}\boldsymbol{w}_\mathrm{a} \quad (28)$$

still satisfies the constraint. In Fig. 3, the quiescent path is in charge of setting up the beamforming weights with common nulls, while the adaptation path is in charge of eliminating one of the two signal components. In the sequel, the design of each path is described.

$$\mathrm{Re}[\boldsymbol{R}_{ss}] = \begin{bmatrix} \sigma_1^2 & \sigma_1^2\rho_1\cos(\Delta\psi_{12}) & 0 & 0 \\ \sigma_1^2\rho_1\cos(\Delta\psi_{12}) & \sigma_1^2\rho_1^2 & 0 & 0 \\ 0 & 0 & \sigma_3^2 & \sigma_3^2\rho_3\cos(\Delta\psi_{34}) \\ 0 & 0 & \sigma_3^2\rho_3\cos(\Delta\psi_{34}) & \sigma_3^2\rho_3^2 \end{bmatrix} \quad (26)$$

*3.2.1 Design of the Quiescent path:* The quiescent path is designed for the purpose of setting up the three quiescent weights $\boldsymbol{w}_{\text{qi}}$ that have common nulls. The constraint equation for each quiescent weight is expressed as

$$\boldsymbol{C}_i^H \boldsymbol{w}_{\text{qi}} = \boldsymbol{f}, \quad i = 1, 2, 3 \tag{29}$$

where $\boldsymbol{C}_i$ is the constraint matrix, a column of which represents each linear constraint and $i$ denotes the beam index [upper beam ($i = 1$), centre beam ($i = 2$) and lower beam ($i = 3$), respectively]. Each element of $\boldsymbol{f}$ denotes the response of the constraint. We propose that the number of constraints should be $M-2$. Therefore the constraint matrix $\boldsymbol{C}_i$ has the rank deficiency of two and we can define the blocking matrix $\boldsymbol{B}_i$ (rank of two) for the adaptive beamforming. On the other hand, the conventional 3-D BDML method utilises $M$ constraints in constructing the orthogonal DFT beams. Therefore it is impossible to set up an adaptation path in the conventional 3-D BDML. We also propose that the $j$th column of all constraint matrices $\boldsymbol{c}_j$ should be an array response vector of $\varphi_j$ that can be expressed as

$$\begin{aligned}\boldsymbol{c}_j &= \boldsymbol{a}(\varphi_j) \\ &= [\mathrm{e}^{-\mathrm{j}(M/2-1/2)\varphi_j},\ \mathrm{e}^{-\mathrm{j}(M/2-3/2)\varphi_j},\ \ldots,\ \mathrm{e}^{\mathrm{j}(M/2-3/2)\varphi_j}, \\ &\quad \mathrm{e}^{\mathrm{j}(M/2-1/2)\varphi_j}]^{\mathrm{T}}\end{aligned} \tag{30}$$

where $\varphi_j$ is the phase of the signal to be nulled or steered. Note that $\mathbf{c}_j$ is also conjugate centro-symmetric.

We propose to use the $(M-2)$-dimensional constraint response vector as $\boldsymbol{f} = [1, 0, \ldots, 0]^{\mathrm{T}}$. Then, the first element of $\boldsymbol{f}$ is the single unity gain to be applied in the steering direction, and the other elements correspond to the nullifying direction. As for the centre beam ($i = 2$), we propose to locate the phases of the signals to be nulled uniformly as

$$\varphi_j = \frac{2\pi}{M} j, \quad j = 2, 3, \ldots, M-2 \tag{31}$$

where $\varphi_j$ is the phase of the $j$th constraint, and to steer the beam to the boresight ($\varphi_1 = 0$). Next, we propose to space out the adjacent beams (upper beam and lower beam) with the amount of $2\pi/M$, and hence, we obtain $C_1$ and $C_3$. From (29) and [27], the quiescent weight of each beam is represented as

$$\boldsymbol{w}_{\text{qi}} = \boldsymbol{C}_i (\boldsymbol{C}_i^H \boldsymbol{C}_i)^{-1} \boldsymbol{f}, \quad i = 1, 2, 3 \tag{32}$$

There are $M-5$ common out-of-band nulls in each beamforming weight which are exploited to reduce the order of the polynomial equation for the estimation. Figs. 4*a*–*c* show the phases of the signals to be nulled and steered for each beam and Fig. 4*d* shows the common nulls, when $M$ is set to 24.

*3.2.2 Design of the adaptation path:* The adaptation path is designed for the purpose of reducing the dimension of the signal space by eliminating one of the two objects from the sample covariance matrix, and hence, the two echoes from the remaining object can be localised with three beams. After forming the quiescent weight with the constraint matrix, two nulls among the four remaining nulls, which have indeterminate locations in the constraint, are

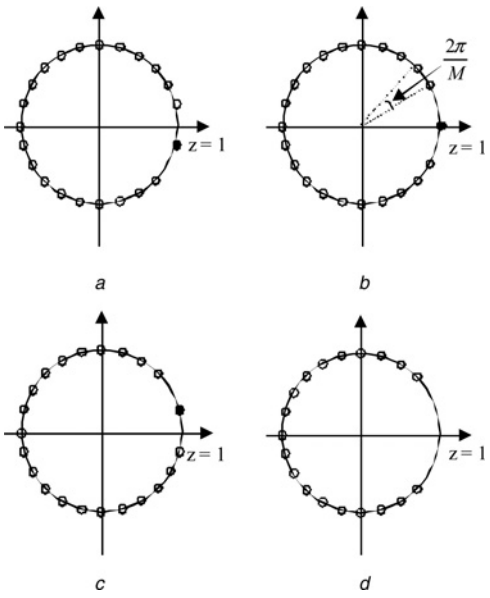


**Fig. 4** *Location of the phases to be nulled (◦) and steered (•) at each beam and the common nulls*

*a* Lower beam
*b* Centre beam
*c* Upper beam
*d* Common nulls

employed for the elimination. First, the blocking matrices $\boldsymbol{B}_i$'s for the three beams are determined according to the corresponding constraint matrix as follows [27]

$$\boldsymbol{B}_1 = \left[\boldsymbol{a}(0) \quad \boldsymbol{a}\left(\frac{4\pi}{M}\right)\right] \in \text{null}(\boldsymbol{C}_1) \tag{33}$$

$$\boldsymbol{B}_2 = \left[\boldsymbol{a}\left(-\frac{2\pi}{M}\right) \quad \boldsymbol{a}\left(\frac{2\pi}{M}\right)\right] \in \text{null}(\boldsymbol{C}_2) \tag{34}$$

$$\boldsymbol{B}_3 = \left[\boldsymbol{a}\left(-\frac{4\pi}{M}\right) \quad \boldsymbol{a}(0)\right] \in \text{null}(\boldsymbol{C}_3) \tag{35}$$

Rewriting (28), the beamforming weight at the GSC output for each beam can be expressed as

$$\boldsymbol{w}_{\text{G}i} = \boldsymbol{w}_{\text{q}i} - \boldsymbol{B}_i \boldsymbol{w}_{\text{a}i}, \quad i = 1, 2, 3 \tag{36}$$

where $i$ denotes the beam index.

Now, we design the adaptation weights. Note that the location of the nulls defined in (31) does not change with these adaptation weights because this adaptation is accomplished in the null space of $\boldsymbol{C}$. In the proposed method, the adaptation weights are designed to extract and eliminate the LPC of the data covariance matrix; that is, the covariance matrix of the data received by the array elements. Therefore the extraction block in Fig. 3 is added to modify the original GSC. Since there are two independent signal components, the data covariance matrix $\boldsymbol{R}_{xx}$ can be expressed as

$$\boldsymbol{R}_{xx} = [\boldsymbol{u}_1\ \boldsymbol{u}_2 \ldots] \begin{bmatrix} \lambda_1 & & \\ & \lambda_2 & \\ & & \ddots \end{bmatrix} \begin{bmatrix} \boldsymbol{u}_1^H \\ \boldsymbol{u}_2^H \\ \vdots \end{bmatrix} \tag{37}$$




doi: 10.1049/iet-rsn.2010.0163

where $\lambda_1$ and $\lambda_2$ are the first and the second largest eigenvalues and $\boldsymbol{u}_1$ and $\boldsymbol{u}_2$ are eigenvectors associated with $\lambda_1$ and $\lambda_2$, respectively. Then, the beamspace data covariance matrix $\boldsymbol{R}_{bb}$ can be expressed as

$$\boldsymbol{R}_{bb} = \boldsymbol{W}_{\mathrm{G}}^H[\boldsymbol{u}_1\ \boldsymbol{u}_2 \ldots]\begin{bmatrix}\lambda_1 & & \\ & \lambda_2 & \\ & & \ddots\end{bmatrix}\begin{bmatrix}\boldsymbol{u}_1^H \\ \boldsymbol{u}_2^H \\ \vdots\end{bmatrix}\boldsymbol{W}_{\mathrm{G}} \quad (38)$$

where $\boldsymbol{W}_{\mathrm{G}} = [\boldsymbol{w}_{\mathrm{G1}}\ \ \boldsymbol{w}_{\mathrm{G2}}\ \ \boldsymbol{w}_{\mathrm{G3}}] \in \mathbb{C}^{M\times 3}$. We propose to design $\mathbf{W}_{\mathrm{G}}$ to reduce the dimension of the signal subspace as follows

$$\boldsymbol{R}_{bb} = \boldsymbol{W}_{\mathrm{G}}^H[\boldsymbol{u}_2 \ldots]\begin{bmatrix}\lambda_2 & \\ & \ddots\end{bmatrix}\begin{bmatrix}\boldsymbol{u}_2^H \\ \vdots\end{bmatrix}\boldsymbol{W}_{\mathrm{G}} \quad (39)$$

The equality holds if $\boldsymbol{u}_1^H\boldsymbol{W}_{\mathrm{G}} = 0$. Therefore the adaptation weight of each beam is determined from the following minimisation problem

$$\min_{\boldsymbol{w}_{\mathrm{G}i}}\|\boldsymbol{u}_1^H\boldsymbol{w}_{\mathrm{G}i}\|^2 = \min_{\boldsymbol{w}_{\mathrm{G}i}}\boldsymbol{w}_{\mathrm{G}i}^H\boldsymbol{P}_1\boldsymbol{w}_{\mathrm{G}i} \quad (40)$$

$$= \min_{\boldsymbol{w}_{ai}}[\boldsymbol{w}_{\mathrm{q}i} - \boldsymbol{B}_i\boldsymbol{w}_{\mathrm{a}i}]^H\boldsymbol{P}_1[\boldsymbol{w}_{\mathrm{q}i} - \boldsymbol{B}_i\boldsymbol{w}_{\mathrm{a}i}],$$

$$i = 1, 2, 3 \quad (41)$$

where $\boldsymbol{P}_1$ is the LPC of the data covariance matrix and can be expressed as

$$\boldsymbol{P}_1 = \lambda_1\boldsymbol{u}_1\boldsymbol{u}_1^H \quad (42)$$

In order to obtain $\boldsymbol{P}_1$, we use the sample covariance matrix of the received data $\hat{\boldsymbol{R}}_{xx} = (1/N)\Sigma_{n=1}^{N}\boldsymbol{x}(n)\boldsymbol{x}^H(n)$ because the ensemble covariance matrix $\boldsymbol{R}_{xx}$ is unknown. The largest eigenvalue can be obtained by the power method or Lanczos method which requires a much lower computational load than full eigendecomposition [28] [We advise the readers to use the Lanczos method (or its variations for faster implementation [29]) because the computational load of the power method is increased if the initial point for the eigenvector is inadequate or $\lambda_2$ is close to $\lambda_1$. The Lanczos method exhibits a faster convergence rate than the power method [28].].

The minimisation problem in (41) is a convex optimisation problem. Taking the differentiation to the objective function (41), we obtain

$$[\boldsymbol{B}_i^H\boldsymbol{P}_1\boldsymbol{B}_i]\boldsymbol{w}_{\mathrm{a}i} = \boldsymbol{B}_i^H\boldsymbol{P}_1\boldsymbol{w}_{\mathrm{q}i}, \quad i = 1, 2, 3 \quad (43)$$

While determining the adaptation weights by solving (43), one more constraint should be considered. This constraint is that the beamforming weights need to be conjugate centro-symmetric to localise coherent signals [17]. Here, the solution of (43) with this constraint is denoted by $\boldsymbol{w}_{\mathrm{a}i}^o$, which can be expressed as

$$\boldsymbol{w}_{\mathrm{a}i}^o = \begin{bmatrix}\mathrm{Re}\{B_i^H\boldsymbol{P}_1B_i\} \\ \mathrm{Im}\{B_i^H\boldsymbol{P}_1B_i\}\end{bmatrix}^{\dagger}\begin{bmatrix}\mathrm{Re}\{B_i^H\boldsymbol{P}_1w_{\mathrm{q}i}\} \\ \mathrm{Im}\{B_i^H\boldsymbol{P}_1w_{\mathrm{q}i}\}\end{bmatrix}, \quad i = 1, 2, 3 \quad (44)$$

where $()^{\dagger}$ denotes the pseudo inverse. The proof is presented in Appendix 7.1.

From (43), the following equality holds

$$\boldsymbol{B}_i^H\boldsymbol{P}_1(\boldsymbol{w}_{\mathrm{q}i} - \boldsymbol{B}_i\boldsymbol{w}_{\mathrm{a}i}) = \lambda_1\boldsymbol{B}_i^H\boldsymbol{u}_1\boldsymbol{u}_1^H\boldsymbol{w}_{\mathrm{G}i} = [0\ 0]^{\mathrm{T}}, \quad i = 1, 2, 3 \quad (45)$$

Since the two columns in $\boldsymbol{B}_i$ are the array response vectors from different directions, $\boldsymbol{B}_i^H\boldsymbol{u}_1$ is not zero, and hence, we obtain

$$\boldsymbol{u}_1^H[\boldsymbol{w}_{\mathrm{G1}}\ \boldsymbol{w}_{\mathrm{G2}}\ \boldsymbol{w}_{\mathrm{G3}}] = \boldsymbol{u}_1^H\boldsymbol{W}_{\mathrm{G}} = 0 \quad (46)$$

which implies that the LPC is eliminated in the beamspace domain.

The remaining signal component is divided into two in the real part of $\boldsymbol{R}_{bb}$ as shown in Section 3.1, and hence, $\mathrm{Re}[\boldsymbol{R}_{bb}]$ can be expressed as

$$\mathrm{Re}[\boldsymbol{R}_{bb}] = \boldsymbol{W}_{\mathrm{G}}^H[\boldsymbol{u}_{2a}\ \boldsymbol{u}_{2b} \ldots]\begin{bmatrix}\lambda_{2a} & & \\ & \lambda_{2b} & \\ & & \ddots\end{bmatrix}\begin{bmatrix}\boldsymbol{u}_{2a}^H \\ \boldsymbol{u}_{2b}^H \\ \vdots\end{bmatrix}\boldsymbol{W}_{\mathrm{G}} \quad (47)$$

where $\boldsymbol{u}_{2a}$, $\boldsymbol{u}_{2b}$, $\lambda_{2a}$ and $\lambda_{2b}$ denote the eigenvectors and the eigenvalues, respectively, of the real part of the remaining component, $\lambda_2\ \boldsymbol{u}_2\ \boldsymbol{u}_2^H$.

*3.2.3 Orthogonalisation of the beamforming weights:* After building the beamforming weights such that they have the three properties, the orthogonalisation procedure should be followed for the estimation in (4) to be the ML estimation. If the eigenvalue decomposition of $\boldsymbol{W}_{\mathrm{G}}^H\boldsymbol{W}_{\mathrm{G}}$ yields

$$\boldsymbol{W}_{\mathrm{G}}^H\boldsymbol{W}_{\mathrm{G}} = \boldsymbol{V}\Sigma\boldsymbol{V}^H \quad (48)$$

the orthogonalised beamforming weight can be expressed as

$$\boldsymbol{W} = \boldsymbol{W}_{\mathrm{G}}\boldsymbol{V}\Sigma^{-(1/2)} \quad (49)$$

From (46) and (49), it is apparent that the orthogonalised beamforming weight also eliminates the LPC as

$$\boldsymbol{u}_1^H\boldsymbol{W} = 0 \quad (50)$$

Since $\boldsymbol{W}_{\mathrm{G}}$ is conjugate centro-symmetric, $\boldsymbol{W}_{\mathrm{G}}^H\boldsymbol{W}_{\mathrm{G}}$ is a real matrix, and hence, $\boldsymbol{V}$ also becomes a real matrix. The orthogonalisation maintains the conjugate centro-symmetric property because $\boldsymbol{W}^* = \boldsymbol{W}_{\mathrm{G}}^*\boldsymbol{V}\Sigma^{-(1/2)} = \boldsymbol{T}\boldsymbol{W}$, where the superscript $*$ of the matrix $\boldsymbol{W}$ and $\boldsymbol{W}_{\mathrm{G}}$ denotes the elementwise complex conjugate and $\boldsymbol{T}$ is the $M \times M$ reverse permutation matrix (see Appendix 7.1). Furthermore, if $\varphi_j$ is one of the common nulls in $\boldsymbol{W}_{\mathrm{G}}$; that is, $\boldsymbol{W}_{\mathrm{G}}^H\boldsymbol{a}(\varphi_j) = 0$, $\varphi_j$ is also a common null of $\boldsymbol{W}$ as

$$\boldsymbol{W}^H\boldsymbol{a}(\varphi_i) = \Sigma^{-(1/2)}\boldsymbol{V}^H\boldsymbol{W}_{\mathrm{G}}^H\boldsymbol{a}(\varphi_j) = 0 \quad (51)$$

This implies that the common nulls that have already been fixed before the orthogonalisation are not changed. The eliminated component $\boldsymbol{u}_1$ is also removed by the

orthogonalised beamforming weight, which can be shown in a similar way. Therefore we can use the orthogonalised beamforming weight in the estimation process.

The procedure of the proposed method is shown along with that of the conventional 3-D BDML method in Fig. 5. The designing stage of the proposed beamforming weights is highlighted in a shaded box. Each step of the proposed method is represented in a small box, and then, the proposed beamforming weights substitute the weights of the 3-D BDML. The estimation stage is similar to that of the conventional 3-D BDML except for some points. The subsequent subsection is dedicated to the description of the proposed estimation stage, focusing on the difference from the estimation stage of the 3-D BDML.

### 3.3 DOA estimation of four signals

Before describing the DOA estimation process, the relations between the eigenvectors $\boldsymbol{u}_1$, $\boldsymbol{u}_2$ in (37) and array response vectors $\boldsymbol{a}(\phi_i)$, $i = 1, \ldots, 4$ are examined. Since the four signals intermingle in the 2-D signal subspace of $\boldsymbol{R}_{xx}$ as described in Section 3.1, the two signal components in $\boldsymbol{R}_{xx}$ contain all four array response vectors in noiseless condition; that is, $\boldsymbol{u}_1$ and $\boldsymbol{u}_2$ can be represented by the span of $\boldsymbol{a}(\phi_i)$, $i = 1, \ldots, 4$. Here, for a conceptual explanation, we assume that $\boldsymbol{a}(\phi_i)$, $i = 1, \ldots, 4$ are mutually orthogonal. Then, one of $\boldsymbol{u}_1$ and $\boldsymbol{u}_2$ can be represented by the span of $\boldsymbol{a}(\phi_1)$ and $\boldsymbol{a}(\phi_2)$, and the other can be represented by the span of $\boldsymbol{a}(\phi_3)$ and $\boldsymbol{a}(\phi_4)$. Here, $\boldsymbol{u}_1$ is eliminated in $\boldsymbol{R}_{xx}$ by the beamforming weights. If, for example, $\mathbf{u}_1$ corresponds to $\boldsymbol{a}(\phi_1)$ and $\boldsymbol{a}(\phi_2)$, $\boldsymbol{a}(\phi_3)$ and $\boldsymbol{a}(\phi_4)$ can be estimated by the 3-D BDML with $\boldsymbol{R}_{xx}$–$\boldsymbol{P}_1$. In addition, since the nulls in the beamforming weights are formed such that $\boldsymbol{u}_1$ is eliminated, $\boldsymbol{a}(\phi_1)$ and $\boldsymbol{a}(\phi_2)$ are also estimated by the 3-D BDML with $\boldsymbol{P}_1$. However, $\boldsymbol{a}(\phi_i)$, $i = 1, \ldots, 4$ are not orthogonal in general, and hence, 3-D BDML with $\boldsymbol{R}_{xx}$ or $\boldsymbol{R}_{xx}$–$\boldsymbol{P}_1$ does not works, which will be shown in Section 4. The derivation for the solution in a general case is given below.

First, remind that the 1-D projection vector is denoted by $\boldsymbol{v}$ as in (12). By the definition in (7) and (8), $\boldsymbol{v}$ is orthogonal to the signal space in the 3-D beamspace domain. As signal space is reduced to be 2-D as in (47), there exists a vector which is orthogonal to the signal space in the 3-D beamspace domain, and hence, $\boldsymbol{v}$ can be obtained. Moreover, $\boldsymbol{v}$ is orthogonal to the product of the beamforming weight and the array response vectors for all the four directions; that is

$$\boldsymbol{v}^{\mathrm{T}}\boldsymbol{W}^{H}\boldsymbol{a}(\phi_i) = 0, \quad i = 1, 2, 3, 4 \tag{52}$$

The proof of (52) is provided in Appendix 7.2. This indicates that the orthogonality between $\boldsymbol{v}$ and the span of the four beamspace array response vectors, $\boldsymbol{W}^{H}\boldsymbol{a}(\phi_i)$, is preserved in spite of the elimination of the LPC. Therefore all the four DOAs of the signals are estimated by solving (52).

Specifically, with the substitution of $\boldsymbol{v} = [v_1, v_2, v_3]$ in (52) and some manipulations, we obtain

$$\mathrm{e}^{-\mathrm{j}(M/2-1/2)\phi_i}(v_1\boldsymbol{w}_1^{H}\boldsymbol{z}(z_i) + v_2\boldsymbol{w}_2^{H}\boldsymbol{z}(z_i) + v_3\boldsymbol{w}_3^{H}\boldsymbol{z}(z_i)) = 0, \quad i = 1, 2, 3, 4 \tag{53}$$

where $\boldsymbol{w}_1$, $\boldsymbol{w}_2$ and $\boldsymbol{w}_3$ are the columns of $\boldsymbol{W}$ which represent the beamforming weights of the lower, centre, and upper beams, respectively, and $i$ represents the index of the DOAs. The $M \times 1$ complex vector $\boldsymbol{z}(z_i)$ is represented as

$$\boldsymbol{z}(z_i) = [1, \ z_i, \ z_i^2, \ \ldots, \ z_i^{M-1}]^{\mathrm{T}} \tag{54}$$

with

$$z_i = \mathrm{e}^{\mathrm{j}\phi_i}, \quad i = 1, 2, 3, 4 \tag{55}$$

Then, $z_i$'s are the four roots of the $(M-1)$th order polynomial, $\boldsymbol{e}(z)$, which is defined as

$$\boldsymbol{e}(z) \triangleq v_1\boldsymbol{w}_1^{H}\boldsymbol{z}(z) + v_2\boldsymbol{w}_2^{H}\boldsymbol{z}(z) + v_3\boldsymbol{w}_3^{H}\boldsymbol{z}(z) \tag{56}$$

Since we have designed the beamforming weights to have $(M-5)$ common nulls, each term of (56) still has the common roots corresponding to the common nulls, and hence, (56) can be represented as

$$\boldsymbol{e}(z) = \left[\prod_{k=1}^{M-5}(z - r_k)\right]\boldsymbol{q}(z) \tag{57}$$

$$\triangleq \boldsymbol{d}(z)\boldsymbol{q}(z) \tag{58}$$

where $\boldsymbol{d}(z)$ is an $(M-5)$th order polynomial that represents the product of the common root term. Furthermore, $\boldsymbol{q}(z)$ is a quotient term which is a quartic polynomial because there are four uncommon nulls. Thus, we can estimate the DOAs by solving $\boldsymbol{q}(z) = 0$. The way to obtain the coefficients of $\boldsymbol{q}(z)$ is provided in Appendix 7.3. After finding out the coefficients, the equation, $\boldsymbol{q}(z) = 0$ can be solved using Ferrari's method, and the solutions represent the estimated DOAs of the two objects.

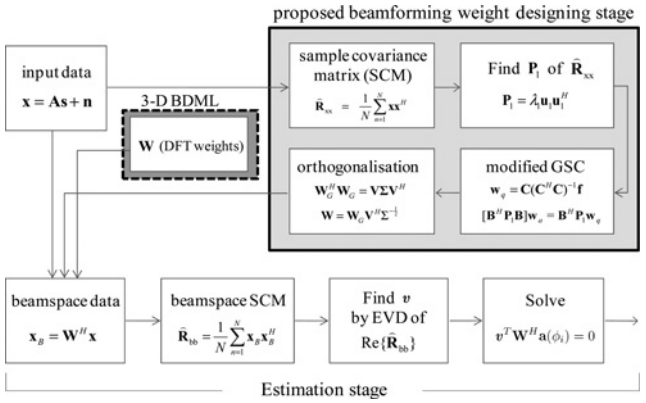


**Fig. 5** *Overall procedure of the conventional and proposed methods ($\lambda_1$: the largest eigenvalue of $\hat{\boldsymbol{R}}_{xx}$, $\boldsymbol{u}_1$: eigenvector associated with $\lambda_1$, $v$: eigenvector associated with the largest eigenvalue of Re[$\hat{\boldsymbol{R}}_{bb}$])*

## 4 Simulations

In this section, we compare the performance of the proposed method to those of the conventional methods by numerical simulations. In all the following simulations, a ULA with $M = 24$ element was considered in the presence of two objects with $N = 10$ snapshots. In the beamspace domain estimation, the accuracy depends on the DOAs of the signals [17]. Therefore in the first simulation, we demonstrate the averaged estimation error over the varying DOAs of the two objects to compare the overall performances. The estimation error is calculated as the




doi: 10.1049/iet-rsn.2010.0163

difference between the true DOA and the estimated DOA of the primary object through the direct path.

The direct echoes from the two objects were assumed to have DOAs varying from $\theta_1 = 1^\circ$ to $\theta_1 = 5^\circ$ with a $1^\circ$ step, and the DOAs of the specular echoes were assumed to be the negative value of the direct DOAs. With this DOA setting, the angular separation between the direct and specular echoes of the each object varies approximately from 0.42 to 2.1 times the nominal 3-dB beamwidth. The angular separation between the two objects varies from 0.21 bandwidths to 0.84 bandwidths. This DOA setting is exactly the same as that in [20]. In addition, the primary object was assumed to be a target, which corresponds to the Swerling model II [25]. Therefore $\alpha_1$, the amplitude of direct echo in (19), was assumed to be a Rayleigh random variable. The second object was assumed to be a jammer, the direct echo of which had a constant amplitude for all snapshots [30].

In the first simulation, we assumed a smooth sea for the reflecting surface. The magnitudes of the reflection coefficients $\rho_1$ and $\rho_3$ were chosen to be 0.9 that is a practical value for the smooth sea surface in a radar system [31]. The diffuse reflection can be neglected in such an environment. Table 1 demonstrates the averaged root mean square (RMS) error with respect to the phase difference between the direct and specular echoes using various methods. The signal-to-noise ratio (SNR) for the direct echo of the primary object and the jammer-to-noise ratio (JNR) for the direct echo of the secondary object was assumed to be 20 dB. The two phase differences ($\Delta\psi_{12}$ and $\Delta\psi_{34}$) were assumed to be the same. The RMS was computed from the results of 10 000 independent trials. The conventional methods considered in this simulation result are the conventional 3-D BDML, the beamspace root-MUSIC with five DFT beams (BR-MUSIC 5), and the 3-D BDML with $\boldsymbol{P}_1$ (or $\boldsymbol{R}_{xx}$–$\boldsymbol{P}_1$). The third method is included to show that the four array response vectors are not mutually orthogonal, and thus, the estimation cannot be accomplished by the 3-D BDML with $\boldsymbol{P}_1$ or $\boldsymbol{R}_{xx}$–$\boldsymbol{P}_1$. Table 2 shows the results of the similar numerical simulation, when the dispersed out-of-band interference was added to the above simulation environment. The dispersed interference is assumed to approach from the varying DOA between $16^\circ$ and $18^\circ$ for every sample. The INR of the out-of-band interference was assumed to be 5 dB. When the out-of-band interference does not exist, the proposed method exhibits the minimum RMS error for the most phase differences values, as can be seen from Table 1. When phase difference is $10^\circ$, the performance of the proposed method was slightly worse than that of the BR-MUSIC 5 but the difference is very small. It can be seen from Table 2 that, if the out-of-band interference exists, the differences between the RMS errors of the proposed method and those of the conventional methods become larger compared to the case in Table 1. With the addition of the out-of-band interference, the RMS error of the conventional BR-MUSIC 5 is increased by 30 to 40%. However, the RMS error of the proposed method is increased 25 to 35%, and eventually, exhibits an RMS error decreased by 2 to 7% compared to that of the conventional BR-MUSIC 5.

Fig. 6 demonstrates the RMS error with respect to the SNR for the direct echo of the primary object approaching from the DOA of $\theta_1 = 1^\circ$. The direct echo of the secondary object was assumed to have the DOA of $\theta_3 = 3^\circ$ with an JNR of 20 dB. As for the phase difference, the performance of the beamspace domain low angle tracking is the best when $\Delta\psi = 90^\circ$ and the worst when $\Delta\psi = 10^\circ$ [20], which is in line with the results shown in Tables 1–3. To cope with the phase difference, the frequency diversity method [20] has been proposed to overcome this problem. As for this simulation, we assumed that $\Delta\psi_{12} = \Delta\psi_{34} = 45^\circ$. The RMS error of proposed method and the conventional BR-MUSIC 5 are compared with each other in Fig. 6. The RMS error levels of the other conventional methods are much higher than that of the proposed methods (they are above $1.5^\circ$), and hence, is omitted. Fig. 7 shows the results of the similar numerical simulation when the dispersed out-of-band interference exists. The DOA and the INR of the dispersed interference are the same as those in Table 2, respectively. Comparing Figs. 6 and 7, we can see that the proposed method is slightly better than the BR-MUSIC 5 when there is no out-of-band interference. However, when the out-of-band interference exists, the difference between the RMS error of the proposed method and those of the conventional methods increases. The RMS error of proposed method drops around 15% as the SNR is increased from 20 to 25 dB.

Next, we assume the rougher sea surface by introducing the diffuse components in the reflections from the two objects.

**Table 1** Averaged RMS error with respect to the phase difference when out-of-band interference does not exist (smooth sea surface)

| Phase difference, deg | 10 | 30 | 50 | 70 | 90 | 110 | 130 | 150 | 170 |
|---|---|---|---|---|---|---|---|---|---|
| 3-D BDML | 21.195 | 7.730 | 4.517 | 2.837 | 2.170 | 1.765 | 1.673 | 1.537 | 1.878 |
| 3-D BDML with $\boldsymbol{P}_1$ (or $\boldsymbol{R}_{xx}$–$\boldsymbol{P}_1$) | 2.429 | 1.948 | 1.663 | 1.480 | 1.317 | 1.118 | 0.954 | 0.816 | 0.924 |
| BR-MUSIC 5 | *0.664* | 0.407 | 0.327 | 0.291 | 0.280 | 0.288 | 0.325 | 0.409 | 0.653 |
| proposed | 0.664 | *0.404* | *0.323* | *0.289* | *0.279* | *0.287* | *0.325* | *0.409* | *0.652* |

The smallest RMS is marked by italics characters (using the values before rounding)

**Table 2** Averaged RMS error with respect to the phase difference when out-of-band interference exists (smooth sea surface)

| Phase difference, deg | 10 | 30 | 50 | 70 | 90 | 110 | 130 | 150 | 170 |
|---|---|---|---|---|---|---|---|---|---|
| 3-D BDML | 21.302 | 7.717 | 4.499 | 2.861 | 2.132 | 1.884 | 1.710 | 1.544 | 1.912 |
| 3-D BDML with $\boldsymbol{P}_1$ (or $\boldsymbol{R}_{xx}$–$\boldsymbol{P}_1$) | 2.420 | 1.942 | 1.659 | 1.485 | 1.318 | 1.118 | 0.962 | 0.819 | 0.935 |
| BR-MUSIC 5 | *0.838* | 0.569 | 0.450 | 0.390 | 0.368 | 0.375 | 0.427 | 0.567 | 0.861 |
| proposed | 0.844 | *0.547* | *0.425* | *0.369* | *0.352* | *0.367* | *0.423* | *0.553* | *0.826* |

The smallest RMS is marked by italics characters

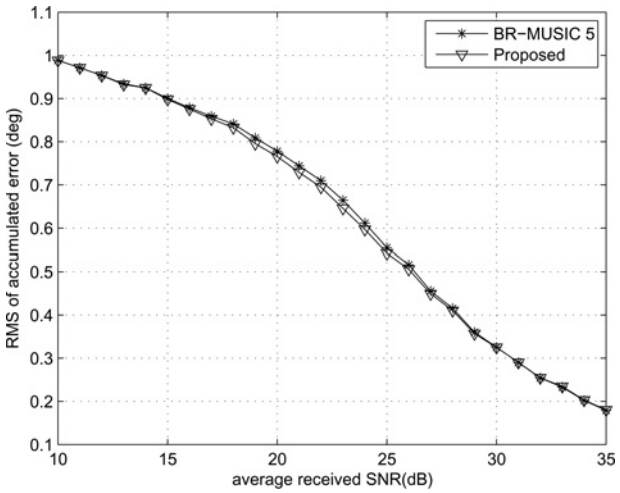


**Fig. 6** *RMS error with respect to the SNR without out-of-band interference (smooth sea surface)*

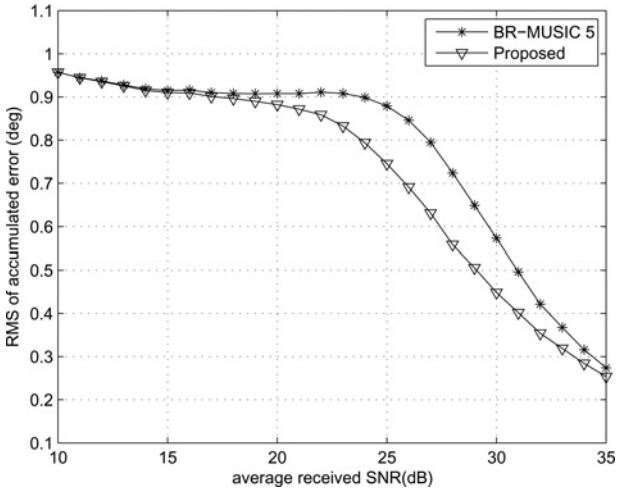


**Fig. 7** *RMS error with respect to the SNR with out-of-band interference (smooth sea surface)*

The magnitude of the reflection coefficients $\rho_1$ and $\rho_3$ was assumed to be dropping to 0.8 due to the rougher surface. The DOAs of the diffuse reflections from the two objects were given under the assumption that the diffuse component was uniformly lying in the region between the objects and the radar but excluding the first Fresnel zone [32]. Here, simulation parameters are as follows: the height of the L-band radar is 10 m, the ranges to the two objects are both 10 km, and the RMS of the wave height is 2 m. The other parameters were assumed to be the same as those in the previous simulation. Table 3 exhibits the averaged RMS error with respect to the phase difference between the direct and the specular echoes using various methods. Table 4 exhibits the results of the similar numerical simulation, when the dispersed out-of-band interference exists. Similar to the results when the smooth surface was assumed, the proposed method shows the minimum RMS error at most values of the phase difference regardless of the out-of-band interference. Moreover, the performance difference between the proposed method and the BR-MUSIC 5 becomes noticeable when there is the out-of-band interference. The RMS error of the proposed method is decreased by up to 6% from that of the conventional BR-MUSIC 5, especially when the phase difference is between 30 and 90°.

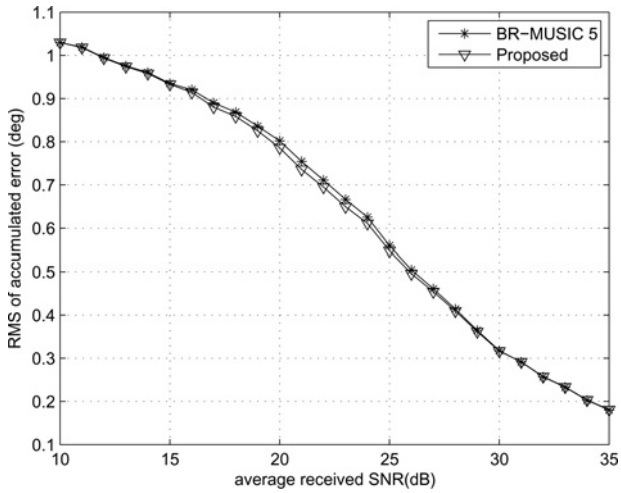


**Fig. 8** *RMS of the averaged error with respect to the SNR without out-of-band interference (rough sea surface)*

Fig. 8 demonstrates the RMS error with respect to the SNR with the same simulation environments as in Fig. 6 except that the diffuse components are included. Fig. 9

**Table 3** RMS of the averaged error with respect to the phase difference when out-of-band interference exists (rough sea surface)

| Phase difference, deg | 10 | 30 | 50 | 70 | 90 | 110 | 130 | 150 | 170 |
|---|---|---|---|---|---|---|---|---|---|
| 3-D BDML | 25.341 | 7.294 | 3.939 | 2.620 | 1.984 | 2.555 | 2.275 | 1.922 | 2.538 |
| 3-D BDML with $\boldsymbol{P}_1$ (or $\boldsymbol{R}_{xx}-\boldsymbol{P}_1$) | 2.413 | 1.950 | 1.668 | 1.494 | 1.323 | 1.114 | 0.933 | 0.697 | 0.845 |
| BR-MUSIC 5 | 0.719 | 0.438 | 0.369 | 0.342 | 0.344 | 0.366 | *0.407* | 0.493 | 0.766 |
| proposed | *0.716* | *0.435* | *0.367* | *0.340* | *0.343* | *0.366* | *0.408* | *0.492* | *0.762* |

The smallest RMS is marked by italics characters (using the values before rounding)

**Table 4** RMS of the averaged error with respect to the phase difference when out-of-band interference exists (rough sea surface)

| Phase difference, deg | 10 | 30 | 50 | 70 | 90 | 110 | 130 | 150 | 170 |
|---|---|---|---|---|---|---|---|---|---|
| 3-D BDML | 25.481 | 7.419 | 3.827 | 2.619 | 2.125 | 2.704 | 2.143 | 2.079 | 2.529 |
| 3-D BDML with $\boldsymbol{P}_1$ (or $\boldsymbol{R}_{xx}-\boldsymbol{P}_1$) | 2.407 | 1.949 | 1.668 | 1.493 | 1.323 | 1.116 | 0.940 | 0.702 | 1.108 |
| BR-MUSIC 5 | *0.826* | 0.579 | 0.468 | 0.426 | 0.423 | 0.447 | 0.508 | 0.650 | 1.070 |
| proposed | 0.831 | *0.558* | *0.443* | *0.408* | *0.411* | *0.443* | *0.506* | *0.643* | *0.988* |

The smallest RMS is marked by italic characters




doi: 10.1049/iet-rsn.2010.0163

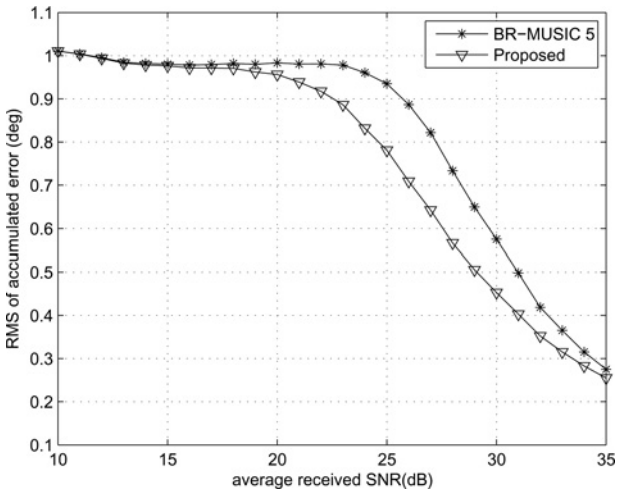


**Fig. 9** *RMS of the averaged error with respect to the SNR with out-of-band interference (rough sea surface)*

demonstrates the results when the dispersed out-of-band interference exists. When the out-of-band interference does not exist, the proposed method shows similar RMS error to that by the BR-MUSIC 5. On the other hand, when the out-of-band interference exists, the RMS error of proposed method is decreased by up to 16% from that of the conventional method.

## 5 Conclusions

This paper presents a low-angle tracking method of two objects in the 3-D beamspace domain by using a linear constraint adaptive array. The proposed method makes it possible to estimate the four DOAs of the signals from two low-angle objects without increasing the number of beams. By the proposed method, a pair of coherent signal components are removed in the beamspace domain covariance matrix. Therefore, the remaining components can be localised by using only three beams. Furthermore, the DOAs of all the four signals are estimated at the end by utilising the properties of the proposed beamforming weights. A linearly constrained adaptive array in the form of a modified GSC grants the necessary properties to the beamforming weights. The common nulls in each beamforming weight elicit a quartic equation that has a closed-form solution. Various numerical simulations exhibit that the proposed method estimates the DOAs more accurately than the conventional methods, especially when dispersed out-of-band interference exists.

## 6 References


1 Sebt, M.A., Sheikhi, A., Nayebi, M.M.: 'Robust low-angle estimation by an array radar', *IET Radar Sonar Navig.*, 2010, **4**, (6), pp. 780–790
2 Barton, D.K.: 'Low angle radar tracking', *Proc. IEEE*, 1974, **62**, (6), pp. 687–704
3 Yu, K.B.: 'Recursive super-resolution algorithm for low-elevation target angle tracking in multipath', *Proc. IEE Radar Sonar Navig.*, 1994, **141**, (4), pp. 223–229
4 Djeddou, M., Belouchrani, A., Aouada, S.: 'Maximum likelihood angle-frequency estimation in partially known correlated noise for low-elevation targets', *IEEE Trans. Signal Process.*, 2005, **53**, (8), pp. 3057–3064
5 Bruder, J.A., Saffold, J.A.: 'Multipath effects on low-angle tracking at millimetre-wave frequencies', *Proc. IEE Radar Signal Process.*, 1991, **138**, (2), pp. 172–184
6 Krim, H., Viberg, M.: 'Two decades of array signal processing research: the parametric approach', *IEEE Signal Process. Mag.*, 1996, **13**, pp. 67–94
7 Sherman, S.M.: 'Monopulse principles and techniques' (Artech House, Dedham, MA, 1984)
8 White, W.D.: 'Low-angle radar tracking in the presence of multipath', *IEEE Trans. Aerosp. Electron. Syst.*, 1974, **AES-10**, pp. 335–352
9 Stoica, P., Sharman, K.C.: 'Maximum likelihood methods for direction-of-arrival estimation', *IEEE Trans. Acoust. Speech Signal Process.*, 1990, **38**, (7), pp. 1132–1143
10 Schmidt, R.O.: 'Multiple emitter location and signal parameter estimation', *IEEE Trans. Antennas Propag.*, 1986, **AP-34**, (3), pp. 276–280
11 Shan, T.-J., Wax, M., Kailath, T.: 'On spatial smoothing for direction-of-arrival estimation of coherent signals', *IEEE Trans. Acoust. Speech Signal Process.*, 1985, **ASSP-33**, (4), pp. 806–811
12 Pillai, S.U., Kwon, B.H.: 'Forward/backward spatial smoothing techniques for coherent signal identification', *IEEE Trans. Acoust. Speech Signal Process.*, 1989, **37**, (1), pp. 8–15
13 Qi, C., Chen, Z., Wang, Y., Zhang, Y.: 'DOA estimation for coherent sources in unknown nonuniform noise fields', *IEEE Trans. Aerosp. Electron. Syst.*, 2007, **43**, (3), pp. 1195–1204
14 Eiges, R., Griffiths, H.D.: 'Mode-space spatial spectral estimation for circular antenna arrays', *Proc. IEE Radar Sonar Navig.*, 1994, **141**, (6), pp. 300–306
15 Kautz, G.M., Zoltowski, M.D.: 'Beamspace DOA estimation featuring multirate eigenvector processing', *IEEE Trans. Signal Process.*, 1996, **44**, (7), pp. 1765–1778
16 Gershman, A.B., Rübsamen, M., Pesavento, M.: 'One- and two-dimensional direction-of-arrival estimation: an overview of search-free techniques', *Signal Process.*, 2010, **90**, (5), pp. 1338–1349
17 Zoltowski, M.D., Kautz, G.M., Silverstein, S.D.: 'Beamspace root-MUSIC', *IEEE Trans. Signal Process.*, 1993, **41**, (1), pp. 344–364
18 Cantrell, B.H., Gordon, W.B., Trunk, G.V.: 'Maximum likelihood elevation angle estimates of radar targets using subapertures', *IEEE Trans. Aerosp. Electron. Syst.*, 1981, **AES-17**, (3), pp. 213–221
19 Haykin, S.: 'Least squares adaptive antenna for angle of arrival estimation', *Proc. IEEE*, 1984, **72**, (4), pp. 528–530
20 Zoltowski, M.D., Lee, T.-S.: 'Maximum likelihood based sensor array signal processing in the beamspace domain for low angle radar tracking', *IEEE Trans. Signal Process.*, 1991, **39**, (3), pp. 656–671
21 Scharf, L.L., McCloud, M.L.: 'Blind adaptation of zero forcing projections and oblique pseudo-inverse for subspace detection and estimation when interference dominates noise', *IEEE Trans. Signal Process.*, 2002, **50**, (12), pp. 2938–2946
22 Tian, Z.: 'Beamspace iterative quadratic WSF for DOA estimation', *IEEE Signal Process. Lett.*, 2003, **10**, (6), pp. 176–179
23 Ward, J.: 'Space-time adaptive processing for airborne radar'. Technical Report 1015, MIT Lincoln Laboratory, Lexington, MA, 1994
24 Lo, T., Litva, J.: 'Use of a highly deterministic multipath signal model in low-angle tracking', *Proc. IEE Radar Signal Process.*, 1991, **138**, (2), pp. 163–171
25 Levanon, N.: 'Radar principles' (Wiley, New York, 1988)
26 Haykin, S.: 'Adaptive filter theory' (Prentice-Hall, Upper Saddle River, NJ, 2002, 4th edn.)
27 Van Trees, H.L.: 'Optimum array processing. Part IV of detection, estimation, and modulation theory' (Wiley, New York, 2002)
28 Golub, G.H., Van Loan, C.F.: 'Matrix computations' (Johns Hopkins University Press, Baltimore, MD, 1996, 3rd edn.)
29 Calvetti, D., Reichel, L., Sorensen, D.C.: 'An implicitly restarted Lanczos method for large symmetric eigenvalue problems', *Electron. Trans. Numer. Anal.*, 1994, **2**, pp. 1–21
30 Raju, K., Ristaniemi, T., Karhunen, J., Oja, E.: 'Jammer suppression in DS-CDMA arrays using independent component analysis', *IEEE Trans. Wirel. Commun.*, 2006, **5**, (1), pp. 77–82
31 Skolnik, M.I.: 'Introduction to radar systems' (McGraw-Hill, New York, 2001, 3rd edn.)
32 Bossé, É., Turner, R.M., Riseborough, E.S.: 'Model-based multifrequency array signal processing for low-angle tracking', *IEEE Trans. Aerosp. Electron. Syst.*, 1995, **31**, (1), pp. 194–210


## 7 Appendix

### 7.1 Solution for the adaptation weight

If the weight is conjugate centro-symmetric, it should satisfy

$$\boldsymbol{w}_{Gi}^{*} = \boldsymbol{T}\boldsymbol{w}_{Gi}, \qquad i = 1, 2, 3 \tag{59}$$

where $\{\}^{*}$ denotes the matrix elementwise complex conjugate and $\boldsymbol{T}$ is the $M \times M$ reverse permutation matrix which can be

expressed as

$$\boldsymbol{T} = \begin{bmatrix} 0 & \cdots & 0 & 1 \\ 0 & \cdots & 1 & 0 \\ & \ddots & & \\ 1 & \cdots & 0 & 0 \end{bmatrix} \tag{60}$$

As aforementioned, since each column of the constraint matrix $\boldsymbol{C}_i$ is an array response vector, the constraint matrix is conjugate centro-symmetric; that is, $\boldsymbol{C}_i^* = \boldsymbol{TC}_i$ and the blocking matrix is also defined to be conjugate centro-symmetric in (33)–(35); that is, $\boldsymbol{B}_i^* = \boldsymbol{TB}_i$. The expression of the quiescent weight (32) shows that $\boldsymbol{w}_{\mathrm{q}i}$ is also conjugate centro-symmetric [29]. From (36) and (59), it becomes

$$\begin{aligned} \boldsymbol{w}_{\mathrm{G}i}^* &= \boldsymbol{w}_{\mathrm{q}i}^* - \boldsymbol{B}_i^* \boldsymbol{w}_{\mathrm{a}i}^* = \boldsymbol{T}\boldsymbol{w}_{\mathrm{q}i} - \boldsymbol{TB}_i \boldsymbol{w}_{\mathrm{a}i}^* \\ &= \boldsymbol{T}\boldsymbol{w}_{\mathrm{G}i} = \boldsymbol{T}\boldsymbol{w}_{\mathrm{q}i} - \boldsymbol{TB}_i \boldsymbol{w}_{\mathrm{a}i} \end{aligned} \tag{61}$$

which means that $\boldsymbol{w}_{\mathrm{a}i}$ should be a real vector. Therefore the way to obtain the adaptation weight is by solving

$$[\boldsymbol{B}_i^H \boldsymbol{P}_1 \boldsymbol{B}_i]\boldsymbol{w}_{\mathrm{a}i} = \boldsymbol{B}_i^H \boldsymbol{P}_1 \boldsymbol{w}_{\mathrm{q}i} \quad s.t.\ \boldsymbol{w}_{\mathrm{a}i} \in \mathbb{R}^{\boldsymbol{M}} \tag{62}$$

Since the rank of $\boldsymbol{P}_1$ is one whereas $[\boldsymbol{B}_i^H \boldsymbol{P}_1 \boldsymbol{B}_i]$ is a $2 \times 2$ matrix, the inverse of $[\boldsymbol{B}_i^H \boldsymbol{P}_1 \boldsymbol{B}_i]$ is not defined. However, (62) can be solved by separating the real part from the imaginary part. Then, the obtained solution, $\boldsymbol{w}_{\mathrm{a}i}^o$ can be expressed as

$$\boldsymbol{w}_{\mathrm{a}i}^o = \begin{bmatrix} \mathrm{Re}\{B_i^H \boldsymbol{P}_1 B_i\} \\ \mathrm{Im}\{B_i^H \boldsymbol{P}_1 B_i\} \end{bmatrix}^{\dagger} \begin{bmatrix} \mathrm{Re}\{B_i^H \boldsymbol{P}_1 w_{\mathrm{q}i}\} \\ \mathrm{Im}\{B_i^H \boldsymbol{P}_1 w_{\mathrm{q}i}\} \end{bmatrix}, \quad i = 1, 2, 3 \tag{63}$$

where $()^{\dagger}$denotes the pseudo inverse.

### 7.2 DOAs and the solution of the quartic equation

The data covariance matrix $\boldsymbol{R}_{xx}$ in a noiseless case can be expressed as (17), which is rewritten by

$$\boldsymbol{R}_{xx} = \boldsymbol{A}(\boldsymbol{\phi})\boldsymbol{R}_{ss}\boldsymbol{A}^H(\boldsymbol{\phi}) \tag{64}$$

By definition in Section 3.1, $s_1(n)$ and $s_2(n)$ are coherent and $s_3(n)$ and $s_4(n)$ are coherent. Therefore the rank of both $\boldsymbol{R}_{ss}$ and $\boldsymbol{R}_{xx}$ are two, and hence, $\boldsymbol{R}_{xx}$ can be expressed as

$$\boldsymbol{R}_{xx} \triangleq \lambda_1 \boldsymbol{u}_1 \boldsymbol{u}_1^H + \lambda_2 \boldsymbol{u}_2 \boldsymbol{u}_2^H \tag{65}$$

where $\lambda_1$ and $\lambda_2$ are the first and the second eigenvalue and $\boldsymbol{u}_1$ and $\boldsymbol{u}_2$ are eigenvectors associated with $\lambda_1$ and $\lambda_2$, respectively. With the equality in (46), the beamspace covariance matrix can be expressed as

$$\begin{aligned} \boldsymbol{R}_{bb} &= \boldsymbol{W}^H \boldsymbol{R}_{\mathrm{xx}} \boldsymbol{W} \\ &= \boldsymbol{W}^H (\lambda_1 \boldsymbol{u}_1 \boldsymbol{u}_1^H + \lambda_2 \boldsymbol{u}_2 \boldsymbol{u}_2^H) \boldsymbol{W} \\ &= \boldsymbol{W}^H (\lambda_2 \boldsymbol{u}_2 \boldsymbol{u}_2^H) \boldsymbol{W} \end{aligned} \tag{66}$$

which means that the rank of $\boldsymbol{R}_{bb}$ is one and $\mathrm{Re}[\boldsymbol{R}_{bb}]$ cannot be a full rank matrix. Therefore the smallest eigenvalue of $\mathrm{Re}[\boldsymbol{R}_{bb}]$ is zero, that is

$$\mathrm{Re}[\boldsymbol{R}_{\mathrm{bb}}]\boldsymbol{v} = \mathrm{Re}[\boldsymbol{W}^H \boldsymbol{A}(\boldsymbol{\phi})\boldsymbol{R}_{ss}\boldsymbol{A}^H(\boldsymbol{\phi})\boldsymbol{W}]\boldsymbol{v} = 0 \tag{67}$$

where $\boldsymbol{v}$ is the eigenvector associated with smallest eigenvalue 0. Since $\boldsymbol{v} \neq \boldsymbol{0}$, the above equation is equivalent to the following equation

$$\boldsymbol{v}^{\mathrm{T}} \mathrm{Re}[\boldsymbol{W}^H \boldsymbol{A}(\boldsymbol{\phi})\boldsymbol{R}_{ss}\boldsymbol{A}^H(\boldsymbol{\phi})\boldsymbol{W}]\boldsymbol{v} = 0 \tag{68}$$

and the conjugate centro-symmetric property of $\boldsymbol{W}$ and $\boldsymbol{A}$ yields

$$\boldsymbol{v}^{\mathrm{T}} \boldsymbol{W}^H \boldsymbol{A}(\boldsymbol{\phi}) \mathrm{Re}[\boldsymbol{R}_{ss}] \boldsymbol{A}^H(\boldsymbol{\phi}) \boldsymbol{W}\boldsymbol{v} = 0 \tag{69}$$

Since $\mathrm{Re}[\boldsymbol{R}_{ss}]$ is full rank unless $\rho_3$ is zero, $\boldsymbol{v}^{\mathrm{T}} \boldsymbol{W}^H \boldsymbol{A}(\boldsymbol{\phi}) = 0$ and the four roots of this equation designate the DOAs from the primary and the secondary objects. If $\rho_3$ is zero, it can be shown easily that the three DOAs from the two objects are included in the four roots of $\boldsymbol{v}^{\mathrm{T}} \boldsymbol{W}^H \boldsymbol{A}(\boldsymbol{\phi}) = 0$. In the presence of the noise, $\boldsymbol{v}$ is the projection to the signal space and the four roots correspond to the least square estimation of the DOAs.

### 7.3 Coefficients of the quartic equation

We can find the coefficients of $\boldsymbol{q}(z)$ in (57) by polynomial division and can express them as

$$q_0 = e_0 \tag{70}$$

$$q_1 = e_1 - d_{M-6} \cdot q_0 \tag{71}$$

$$q_2 = e_2 - d_{M-7} \cdot q_0 - d_{M-6} \cdot q_1 \tag{72}$$

$$q_4 = e_{M-1} \tag{73}$$

$$q_3 = e_{M-2} - d_{M-6} \cdot q_4 \tag{74}$$

where $q_i$, $e_i$ and $d_i$ are the coefficients of the $i$th order term of the $z$ of $\boldsymbol{q}(z)$, $\boldsymbol{e}(z)$ and $\boldsymbol{d}(z)$, respectively. For (71), (72) and (74), the $(M-6)$th coefficient and $(M-7)$th coefficient of $\boldsymbol{d}(z)$ can be obtained by the definition of the $\boldsymbol{d}(z)$ found in (58) and simple manipulation yields

$$d_{M-6} = -\sum_{i=3}^{M-3} r_i \tag{75}$$

$$d_{M-7} = -\frac{1}{2}\left(\left(\sum_{i=3}^{M-3} r_i\right)^2 - \sum_{i=3}^{M-3} r_i^2\right) \tag{76}$$

where $r_3, r_4, \ldots, r_{M-3}$ are the roots of $\boldsymbol{d}(z)$ if we order the roots of $\boldsymbol{e}(z)$ in the phase order (from zero to $2\pi$). The roots of $\boldsymbol{d}(z)$ are the nulls defined in (31), and the sum and the square sum of roots of $\boldsymbol{d}(z)$ can be expressed as follows via simple manipulations

$$\sum_{i=3}^{M-3} r_i = -\left(1 + 2\cos\left(\frac{2\pi}{M}\right) + 4\cos\left(\frac{2\pi}{M}\right)\right) \tag{77}$$

$$\sum_{i=3}^{M-3} r_i^2 = -\left(1 + 2\cos\left(\frac{4\pi}{M}\right) + 4\cos\left(\frac{8\pi}{M}\right)\right) \tag{78}$$




doi: 10.1049/iet-rsn.2010.0163